J. Cent. South Univ. (2020) 27: 3637−3651
DOI: https://doi.org/10.1007/s11771-020-4567-8

Springer

Thermodynamic analysis on tin precipitation behavior in Ti-bearing peritectic steel after magnesium treatment

QU Tian-peng(屈天鹏), WANG De-yong(王德永), WANG Hui-hua(王慧华),
HOU Dong(侯栋), TIAN Jun(田俊)

Shagang School of Iron and Steel, Soochow University, Suzhou 215021, China

Abstract: TiN, which is ubiquitous in Ti-bearing steel, has a critical influence on both the mechanical properties and the welding process of steel, and therefore researche on the precipitation behavior of TiN in molten steel bath is of great significance. In this paper, Ti-bearing peritectic steel was taken as the study object and FactSage was adopted to explore how the precipitation behavior of typical inclusions in steel was affected by the steel composition. Furthermore, microsegregation models were used to analyze the precipitation process of TiN at solidification front, and the calculation results were finally verified by scanning electron microscope (SEM). Research showed that a multitude of dispersed particles of high melting oxide $MgAl_2O_4$ or MgO always existed in molten steel after magnesium treatment. In consideration of the segregation and enrichment of solute elements at the solidification front, the Ohnaka microsegregation model was employed to compute the precipitation during solidification. In the event of the solid fraction reaching 0.95 or more, the concentration product of [Ti][N] at the solidification front exceeded the equilibrium concentration product, then TiN began to precipitate. MgO or $MgAl_2O_4$ cores were generally found in TiN particles of peritectic steel after the magnesium treatment, which was consistent with the thermodynamic calculation results. Moreover, the average size of TiN particles was reduced by approximately 49%. This demonstrated that Mg-rich high melting inclusions were formed after the magnesium treatment, by which the heterogeneous nucleation of TiN was promoted it; therefore, favorable nucleation sites were provided for further refining the high-temperature ferrite phase.

Key words: magnesium treatment; peritectic steel; TiN; heterogeneous nucleation; thermodynamic analysis

Cite this article as: QU Tian-peng, WANG De-yong, WANG Hui-hua, HOU Dong, TIAN Jun. Thermodynamic analysis on tin precipitation behavior in Ti-bearing peritectic steel after magnesium treatment [J]. Journal of Central South University, 2020, 27(12): 3637−3651. DOI: https://doi.org/10.1007/s11771-020-4567-8.

1 Introduction

Microalloyed steel is manufactured usually by adding trace alloying elements (Nb, V, Ti, etc.) to the steel. In the rolling process, deformation induced nano-sized carbides and nitrides are precipitated, which can pin the austenite grain boundaries and enable the fine-grain strengthening mechanism, and thus the strength and toughness of steel are improved. For Ti-bearing microalloyed steel, especially the hypo-peritectic steel with a carbon content of 0.09%−0.17%, peritectic reaction is an important transformation mode in the initial stage of solidification [1−4]. When the primary high-temperature δ-ferrite reacts with the residual molten steel L to form γ-austenite, the difference in crystal structure between δ phase (BCC structure) and γ phase (FCC structure) results in a large volume contraction in the process of solidification, which causes uneven cooling of the primary shell in the mold, and thus shells with different thicknesses and

Foundation item: Projects(51774208, 52074186, U1860205) supported by the National Natural Science Foundation of China
Received date: 2020-08-15; **Accepted date:** 2020-11-23
Corresponding author: WANG Hui-hua, PhD, Associate Professor; Tel: +86-13812759225; E-mail: hhwang@suda.edu.cn; ORCID: https://orcid.org/0000-0001-5664-3265

high cracking susceptibility are formed [5−10]. This cause is considered the root one for the surface cracking of this type of steel.

TiN, which is ubiquitous in Ti-bearing steel, has a critical influence on the properties of steel and on the control of grain size in the heat affected zone during welding. On one hand, TiN is formed from the added Ti, which can strongly react with N, to fix the element N, and the growth of NbN and VN particles is inhibited. The added Ti acts as second phase particles for pinning grain boundaries. On the other hand, in the field of oxide metallurgy, the δ-phase nucleation can be remarkably promoted by the TiN particles as nucleation sites based on the good lattice matching between TiN and ferrite phase. The influence of nitrides and carbides in microalloyed steel on nucleation undercooling was first studied by BRAMFITT [11]. The nucleation effectiveness of typical nitrides and carbides in microalloyed steel was systematically evaluated [12]. The nucleation ability was ranked as (TiN, TiC)>SiC>ZrN>>ZrC>WC, and the calculation formula of two-dimensional lattice misfit was proposed, as shown in Eq. (1). The equation can be used to evaluate the lattice matching relationship between nucleation site and matrix, and further quantitatively determine the relationship between lattice misfit and critical nucleation undercooling.

$$\delta_{(hkl)_{Fe}}^{(hkl)_C}=\frac{1}{3}\sum_{i=1}^{3}\frac{\left|(d_{[uvw]_C^i}\cos\theta)-d_{[uvw]_{Fe}^i}\right|}{d_{[uvw]_{Fe}^i}}\times 100\% \quad (1)$$

where $(hkl)_C$ is the Miller index of carbides and nitrides; $[uvw]_C$ is the internal orientation of the crystal plane $(hkl)_C$; $d_{[uvw]_C^i}$ is the atomic spacing along the crystal orientation $[uvw]_C$; and θ is the angle between $[uvw]_C$ and $[uvw]_{Fe}$.

This method has been widely used to study the heterogeneous nucleation between composite inclusion particles, the heterogeneous nucleation of metal phases by virtue of second-phase particles and the control of coarse structure in heat affected zone during welding. Based on the lattice matching between TiN and ferrite, TiN is used to induce the nucleation of intragranular ferrite during welding in order to enhance the strength and toughness of welded joints [13, 14]. KIMURA et al [15] and FUKUMOTO et al [16] further confirmed that the ratio of equiaxed crystals in as-cast ferritic stainless steel could be significantly increased by the Mg-Ti interaction. PARK et al [17] and KIM et al [18] observed the atomic arrangement on $MgAl_2O_4$-TiN and TiN-δ-Fe interfaces by transmission electron microscope (TEM), which further confirmed that the heterogeneous nucleation of δ phase could be promoted by TiN, while the formation of TiN could be promoted by Mg-bearing particles. An experiment on the Mg-Ti treated ferritic stainless steel SUS430 carried out by ZHANG et al [19] previously discovered that with the increase of Ti content, a large number of Ti particles with a size of 3−5 μm were formed, and the ratio of equiaxed crystals in the ferritic stainless steel rose significantly. When the Ti content was 0.05%, once $(10-15)\times10^{-6}$ Mg was added into the steel, the ratio of equiaxed crystals increased by 20%.

Therefore, how to obtain dispersed TiN particles with a small particle size and a high number density is of great significance to refine the high-temperature microstructure and enhance the mechanical properties of steel. In view of this, a systematical thermodynamic analysis was performed to study the effect of element contents on the precipitation behavior of typical inclusions and the formation of TiN particles at solidification front, and thus a theoretical guidance for the accurate control of TiN particles was provided.

2 Methodology and experiment

Based on the principle of Gibbs free energy minimization, FactSage (V7.3, FactSage, Canada) was used to do systematic thermodynamic calculations for the solidification and phase transformation process of peritectic steel and the precipitation behavior of typical inclusions in the steel. The composition of the steel used in the thermodynamic calculation is shown in Table 1.

The steel used in this study was Ti-bearing hypo-peritectic steel with a carbon content of 0.13%. The composition is shown in Table 1 and the contents of C, Si, Mn, Ti, etc. in the steel were detected using a Spectro-Lab analyzer (NCS Inc., Beijing, China). The element N was detected using an ONH-3000 analyzer (NCS Inc., Beijing, China). And the element Mg was detected using a 6300 ICP analyzer (Varian Medical Systems, UT, USA). The production process was BOF-LF-CC, and the cross section of the continuous casting slab was 220 mm×

Table 1 Composition of the peritectic steel (wt%)

Element	C	Si	Mn	P	S	Al	Ti	Mg	O	N
Before Mg treatment	0.13	0.02	0.34	0.01	0.009	0.0226	0.020	0	0.0032	0.0041
After Mg treatment	0.12	0.03	0.36	0.01	0.007	0.0235	0.018	0.0015	0.0035	0.0039

1860 mm. For studying the effect of magnesium treatment on the hot ductility of peritectic steel, Mg-bearing cored wire (20%Mg-5%Al-75%Fe) was fed into the ladle through a wire feeder after LF refining. The parameters of the continuous casting process were kept the same. Specimens were obtained from the 1/4 area under the slab surface. The specimens before and after magnesium treatment were all dissolved through electrolysis in non-aqueous solution. In order to extract TiN particles from the solution, the inclusion electrolyte was separated out using an HC-2518 centrifuge (Zonkia Inc., Anhui, China) at 10000 r/min. The appearance characteristics of the extracted non-metallic inclusions were analyzed using an SU5000 electron scanning microscope (Hitachi Inc., Tokyo, Japan).

3 Analysis and discussion

3.1 Thermodynamic analysis on solidification process of Ti-bearing peritectic steel

According to the chemical composition in Table 1, the pseudo-binary phase diagram of Fe-C of the steel and the phase change diagram with the temperature interval of 1600 to 300 °C during equilibrium solidification were calculated and plotted, as shown in Figure 1. It reveals that the initial phase of such peritectic steel during solidification was high-temperature δ-ferrite, and the peritectic transformation L+δ→γ occurred when the temperature dropped to the peritectic reaction temperature, while the whole phase change process was described as L→L+δ→L+δ+γ→δ+γ→γ→α+γ→α+Fe_3C. It can be seen that, based on the refinement of high-temperature ferrite through Mg treatment, more attention should be paid to the structure heredity of refined grains before peritectic transformation in order to obtain refined γ phase. If the refined δ phase was inherited to the γ phase, the Mg treatment had the technical potential to improve the hot ductility of peritectic steel. Researchers shall also focus on the precipitation order of inclusions in molten peritectic steel with a given composition; thereby the nucleation in sequence was induced and finally the refinement of δ phase was realized.

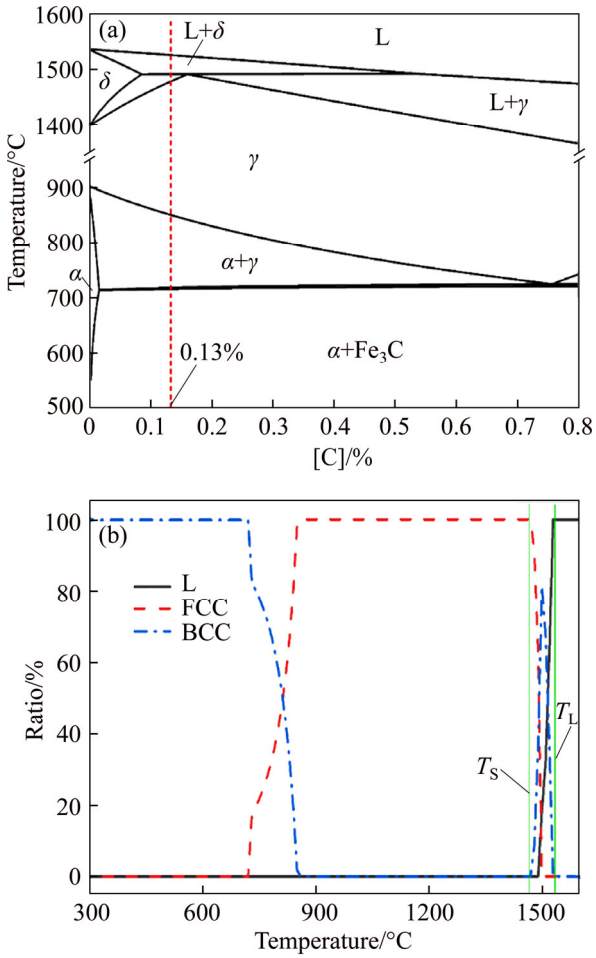

Figure 1 (a) Pseudo-binary phase diagram of Fe-C and (b) Phase transition process of tested steel during equilibrium solidification

3.2 Precipitation behavior analysis on inclusions in steel

To investigate the influence of Mg, Al, O, N, and Ti on the precipitation behavior of typical precipitates in steel, the chemical composition was designed as shown in Table 2, and thermodynamic calculations were performed by FactSage to analyze how the changes of chemical composition influenced the TiN nucleation induced by high melting inclusions in steel.

Table 2 Changes of chemical composition for thermodynamic calculation (wt%)

Case	C	Si	Mn	P	S	Mg	Al	O	Ti	N
1	0.13	0.02	0.34	0.01	0.009	**0.001**	**0.02**	**0.005**	**0.02**	**0.004**
2	0.13	0.02	0.34	0.01	0.009	**0.002**	0.02	0.005	0.02	0.004
3	0.13	0.02	0.34	0.01	0.009	**0.003**	0.02	0.005	0.02	0.004
4	0.13	0.02	0.34	0.01	0.009	**0.004**	0.02	0.005	0.02	0.004
5	0.13	0.02	0.34	0.01	0.009	**0.005**	0.02	0.005	0.02	0.004
6	0.13	0.02	0.34	0.01	0.009	0.001	**0.01**	0.005	0.02	0.004
7	0.13	0.02	0.34	0.01	0.009	0.001	**0.03**	0.005	0.02	0.004
8	0.13	0.02	0.34	0.01	0.009	0.001	**0.04**	0.005	0.02	0.004
9	0.13	0.02	0.34	0.01	0.009	0.001	0.02	**0.003**	0.02	0.004
10	0.13	0.02	0.34	0.01	0.009	0.001	0.02	**0.004**	0.02	0.004
11	0.13	0.02	0.34	0.01	0.009	0.001	0.02	**0.006**	0.02	0.004
12	0.13	0.02	0.34	0.01	0.009	0.001	0.02	0.005	**0.01**	0.004
13	0.13	0.02	0.34	0.01	0.009	0.001	0.02	0.005	**0.03**	0.004
14	0.13	0.02	0.34	0.01	0.009	0.001	0.02	0.005	**0.04**	0.004
15	0.13	0.02	0.34	0.01	0.009	0.001	0.02	0.005	0.02	**0.002**
16	0.13	0.02	0.34	0.01	0.009	0.001	0.02	0.005	0.02	**0.003**
17	0.13	0.02	0.34	0.01	0.009	0.001	0.02	0.005	0.02	**0.005**

3.2.1 Effect of magnesium content

The influence of Mg content in steel on the precipitation behavior of typical precipitates in Ti-bearing peritectic steel is illustrated in Figure 2. The Mg content used for calculation ranged from 10×10^{-6}–50×10^{-6}. As can be seen, the main precipitates formed in the process of equilibrium solidification of such peritectic steel include TiN, TiC, Al_2O_3, $MgAl_2O_4$, AlN and MgO. The change of Mg content in steel has no effect on the precipitation curves of TiN, TiC and AlN, but exerts a direct influence on the precipitation curves of Al_2O_3, $MgAl_2O_4$ and MgO. When the steel contains only 10×10^{-6} Mg, high melting $MgAl_2O_4$ and Al_2O_3 are formed in the high-temperature molten steel, in which $MgAl_2O_4$ is generated prior to Al_2O_3. When the content of Mg turns more than 20×10^{-6}, Al_2O_3 essentially doesn't exist in the molten steel. By comparing the temperature curves of $MgAl_2O_4$ in Figures 2(a) and (b), we know that the Al enters into $MgAl_2O_4$. When the Mg content reaches 30×10^{-6}, MgO begins to form in the high-temperature molten steel, and as the Mg content increases, the curve of $MgAl_2O_4$ moves down and the curve of MgO gradually moves up. This is mainly attributed to the fact that partial $MgAl_2O_4$ was reduced by the Mg added in the molten steel. Therefore, a large number of high melting $MgAl_2O_4$ and MgO inclusion particles are formed in the steel. Based on the good lattice matching between $MgAl_2O_4$/MgO and TiN, it can be predicted that for Ti-bearing peritectic steel, plentiful nucleation sites favorable to TiN nucleation can form in high-temperature molten steel after Mg treatment.

3.2.2 Effect of aluminum content

The influence of Al content in steel on the precipitation behavior of typical precipitates is illustrated in Figure 3, where the Al content changes from 0.01% to 0.04%. As can be seen that, in addition to Ti_3O_5 formed when the Al content is low, the precipitates are still dominated by TiN, TiC, Al_2O_3, $MgAl_2O_4$ and AlN. In the event of constant Mg and O contents in steel, if the Al content is 0.01%, O and Mg first combine with the Al to form stable magnesium-aluminum spinel $MgAl_2O_4$ in molten steel. The surplus O forms Ti_3O_5 in the temperature interval of 1350−1500 °C, but it first generates Al_2O_3 instead of Ti_3O_5 in the case of a high Al content in steel. It should be noted that with the increase of Al content in steel, Ti_3O_5 is reduced, and the amount of TiC precipitation is increased by the dissolved Ti during cooling, which explains why the TiC curve in low-temperature zone slightly moves up. Since the Mg content is constant, the

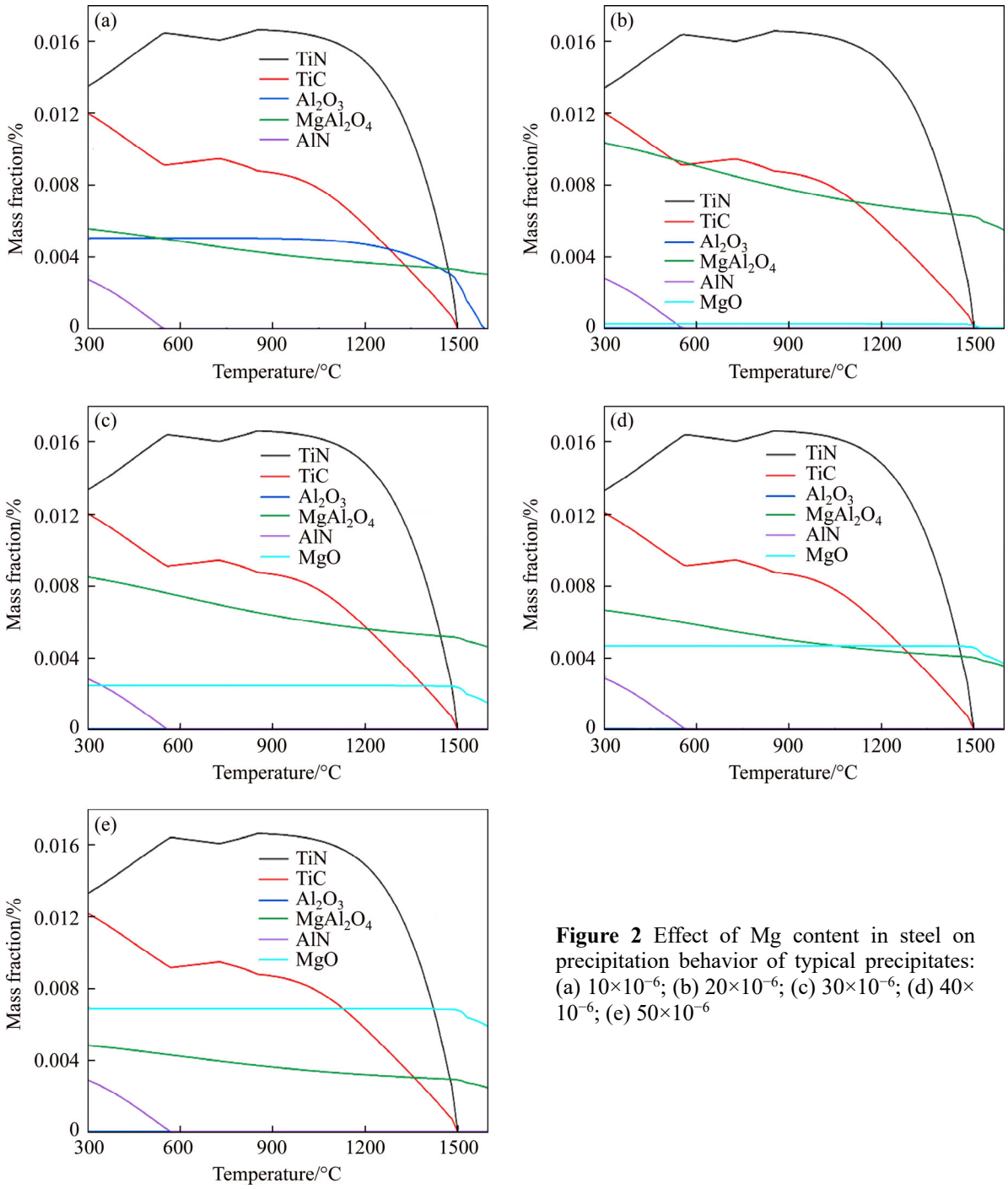

Figure 2 Effect of Mg content in steel on precipitation behavior of typical precipitates: (a) 10×10^{-6}; (b) 20×10^{-6}; (c) 30×10^{-6}; (d) 40×10^{-6}; (e) 50×10^{-6}

$MgAl_2O_4$ curve does not change with the increase of Al content, that is, an Al content of 0.01% is sufficient to form the stable magnesium-aluminum spinel with the dissolved Mg in steel, and the formed spinel can exist stably in high-temperature molten steel. When the Al content is higher than 0.02%, the Al_2O_3 curve turns basically stable, indicating that the reaction between dissolved O and Al has been completed. When the Al content was excessive in steel, $MgAl_2O_4$ and Al_2O_3 are the stable high-melting substances in molten steel, capable of providing effective nucleation sites for TiN precipitation.

3.2.3 Effect of titanium content

Ti is a typical alloying element in microalloyed steel. Nano-sized TiN and TiC particles precipitated in steel are effective precipitates and play the role of pinning grain boundaries during rolling. The influence of Ti content in steel on the precipitation behavior of typical precipitates is illustrated in Figure 4, where the Ti content changes from 0.01% to 0.04%. As can be seen, besides the main

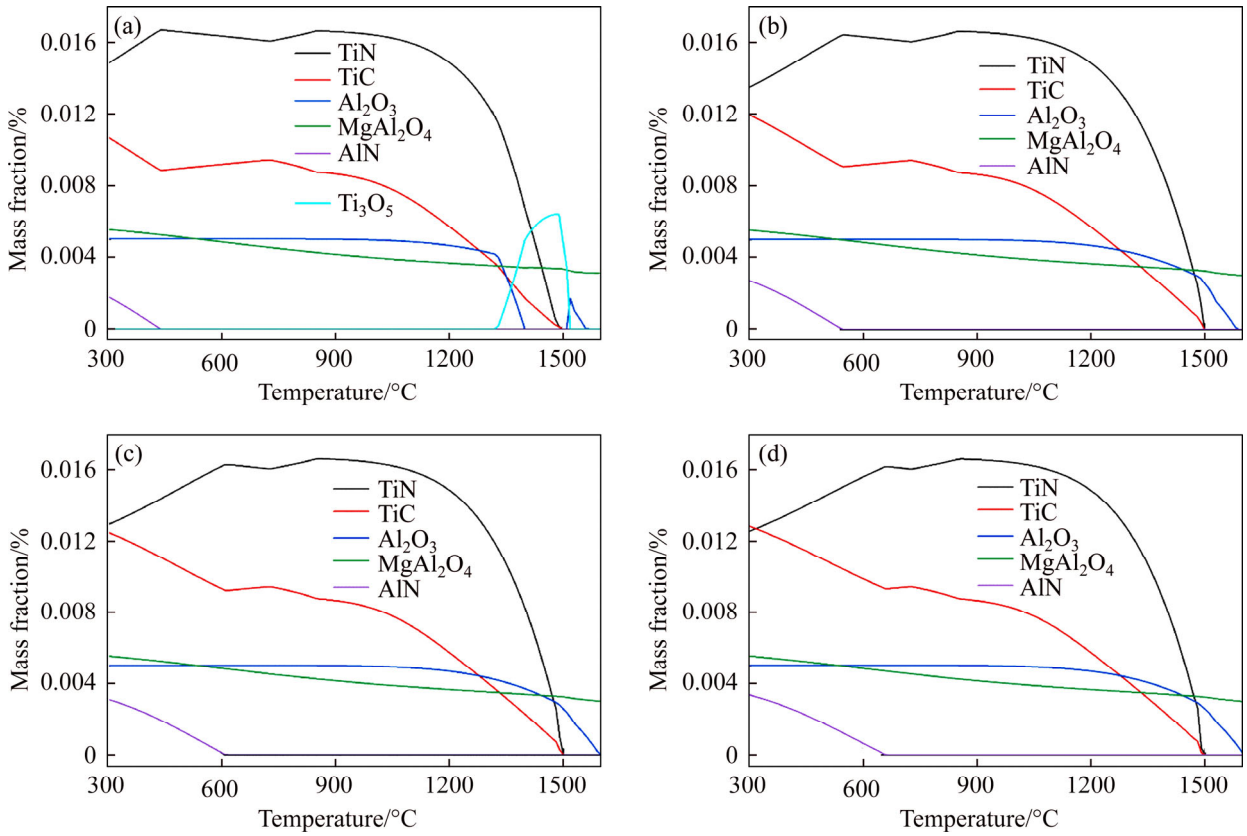

Figure 3 Effect of Al content in steel on precipitation behavior of typical precipitates: (a) 0.01% Al; (b) 0.02% Al; (c) 0.03% Al; (d) 0.04% Al

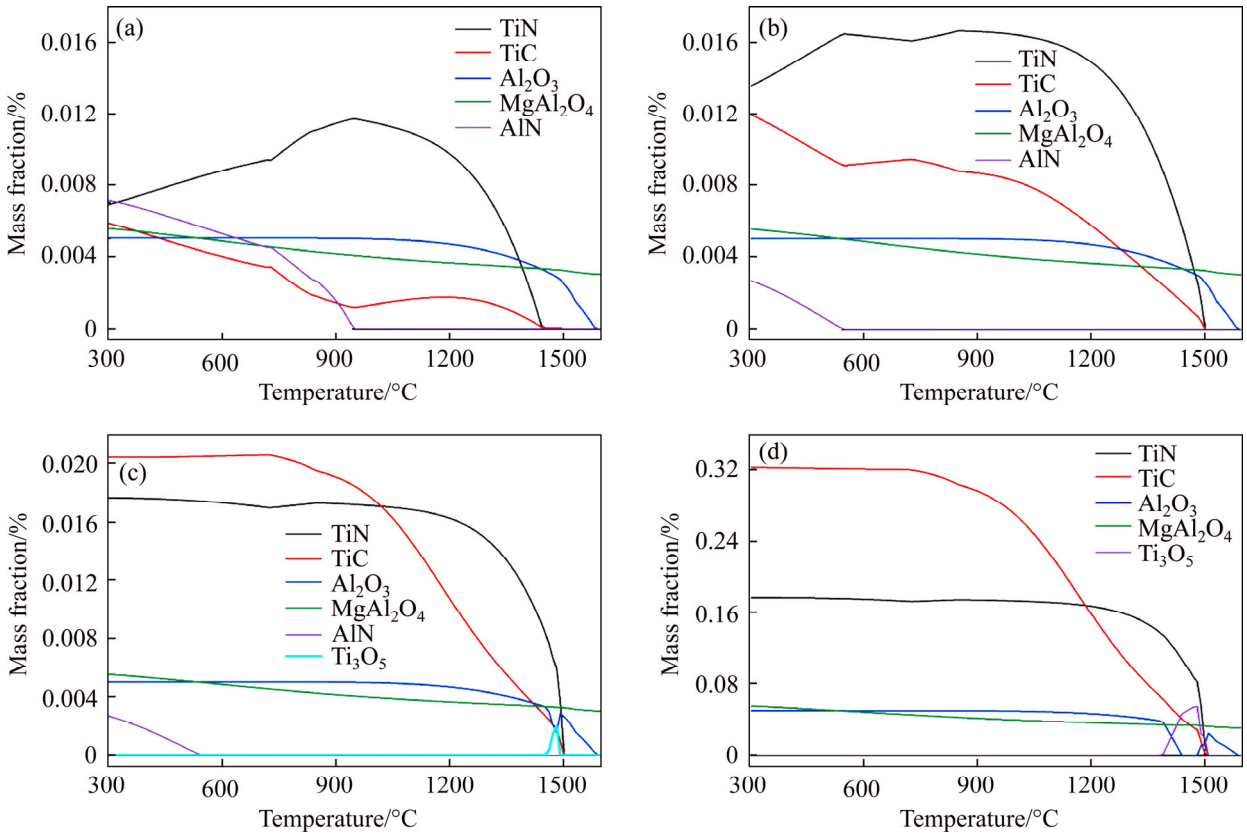

Figure 4 Effect of Ti content in steel on precipitation behavior of typical precipitates: (a) 0.01% Ti; (b) 0.02% Ti; (c) 0.03% Ti; (d) 0.04% Ti

precipitates TiN, TiC, Al_2O_3, $MgAl_2O_4$ and AlN, Ti_3O_5 and Ti_2O_3 are also formed in the event of a high Ti content. The amount of TiN and TiC precipitation grows with the increase of Ti content. When the Ti content is higher than 0.03%, the amount of TiN precipitation turns to be basically stable, while the amount of TiC precipitation continues to increase. Ti is an important element for fixing N in steel, and Figures 4(a)−(d) exhibit that when the Ti content is only 0.01% in steel, TiN is formed from N, and the surplus N combines with Al to produce AlN. It is reflected in Figure 4(a) that AlN begins to precipitate at 950 °C during equilibrium solidification. With the increase of Ti content, the element N combines with Ti to form more TiN, whereas both the precipitation amount and the precipitation temperature of AlN show a downward trend. Once the Ti content to be turns higher than 0.03%, the element N primarily combines with Ti to form TiN, and then AlN will not be produced any more in steel.

Researches show that AlN in steel tends to precipitate at austenite grain boundaries, which leads to grain boundary embrittlement, expands the width of the third brittle zone and has an adverse effect on the hot ductility of slab. Therefore, it is necessary to increase the Ti content in steel to avoid excessive AlN precipitation. When the Ti content rises to more than 0.04%, the excessive Ti in steel reduces Al_2O_3 to form Ti_3O_5 and Ti_2O. Therefore, the Ti content in Ti-bearing microalloyed steel shall be reasonably designed based on the chemical composition of steel. From the perspective of promoting heterogeneous nucleation of TiN, $MgAl_2O_4$ and Al_2O_3 formed in high-temperature molten steel still play an important role, where $MgAl_2O_4$ dominates.

3.2.4 Effect of nitrogen content

N is generally regarded as a harmful element in microalloyed steel, and its content is expected to be minimized. However, from the perspective of heterogeneous nucleation, a reasonable nitrogen content is essential to promote the formation of typical precipitates, in which a large number of fine TiN particles are formed to promote the nucleation of high-temperature δ-ferrite. The influence of N content in steel on the precipitation behavior of typical precipitates is illustrated in Figure 5, where the N content changes from 20×10^{-6} to 50×10^{-6}.

As can be seen that the most significant effect on the TiN and AlN curves is exerted by the change of N content in steel. When the N content is 20×10^{-6}, the resulting stable TiN content is about 0.09%, lower than the TiC content, which is mainly due to the low N content and the excessive Ti combining with C. With the increase of N content in steel, the TiN content rises significantly. With regard to the competition between AlN and TiN for N, TiN is more stable, and that is why the N added in steel first combines with the dissolved Ti to form stable TiN. Once all the dissolved Ti is consumed, excessive N combines with Al to produce AlN and the precipitation temperature of AlN increases gradually. When the N content is increased from 40×10^{-6} to 50×10^{-6}, the initial precipitation temperature of AlN rises from 530 to 750 °C. An adverse effect on the hot ductility can be caused by the precipitation of a large number of AlN particles, which shall be restrained. In view of this, the N content in steel shall be controlled to be less than 40×10^{-6}. Under this condition, a large number of TiN particles have been produced in steel, with the high melting $MgAl_2O_4$ particles precipitating earlier which can induce nucleation, so adequate nucleation sites are available now for refining the high-temperature δ-ferrite.

3.2.5 Effect of oxygen content

Reoxidation of molten steel is required to be strictly controlled in the process of continuous casting of steel to avoid any loss of metallurgical effect of valuable elements in steel caused by excessive oxidation. The influence of oxygen content in steel on the precipitation behavior of typical precipitates is illustrated in Figure 6, where the O content changes from 30×10^{-6} to 60×10^{-6}. As can be seen, the change of O content only has a significant effect on the Al_2O_3 curve. As the O content increases, the Al_2O_3 curve moves up and the precipitation temperature of Al_2O_3 increases gradually. And the high melting substances formed in the molten steel with a high oxygen content are Al_2O_3 and $MgAl_2O_4$. Researches show a high lattice misfit of Al_2O_3 with TiN, which means that Al_2O_3 is not an effective nucleating agent for TiN. Therefore, to ensure uninterrupted casting process and promote heterogeneous nucleation, the O content in steel should be strictly controlled and reduced as far as possible.

It is indicated by the above calculations that stable $MgAl_2O_4$/MgO particles are formed in high-

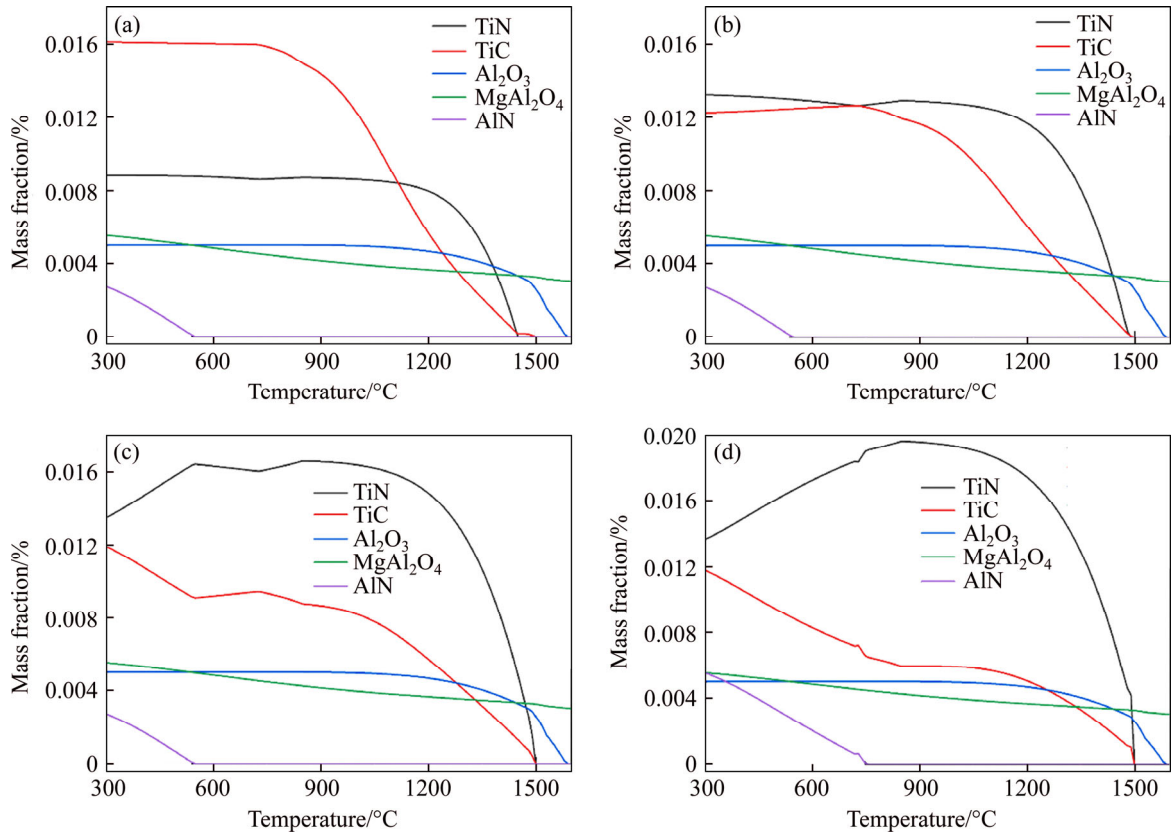

Figure 5 Effect of N content in steel on precipitation behavior of typical precipitates: (a) 20×10^{-6}; (b) 30×10^{-6}; (c) 40×10^{-6}; (d) 50×10^{-6}

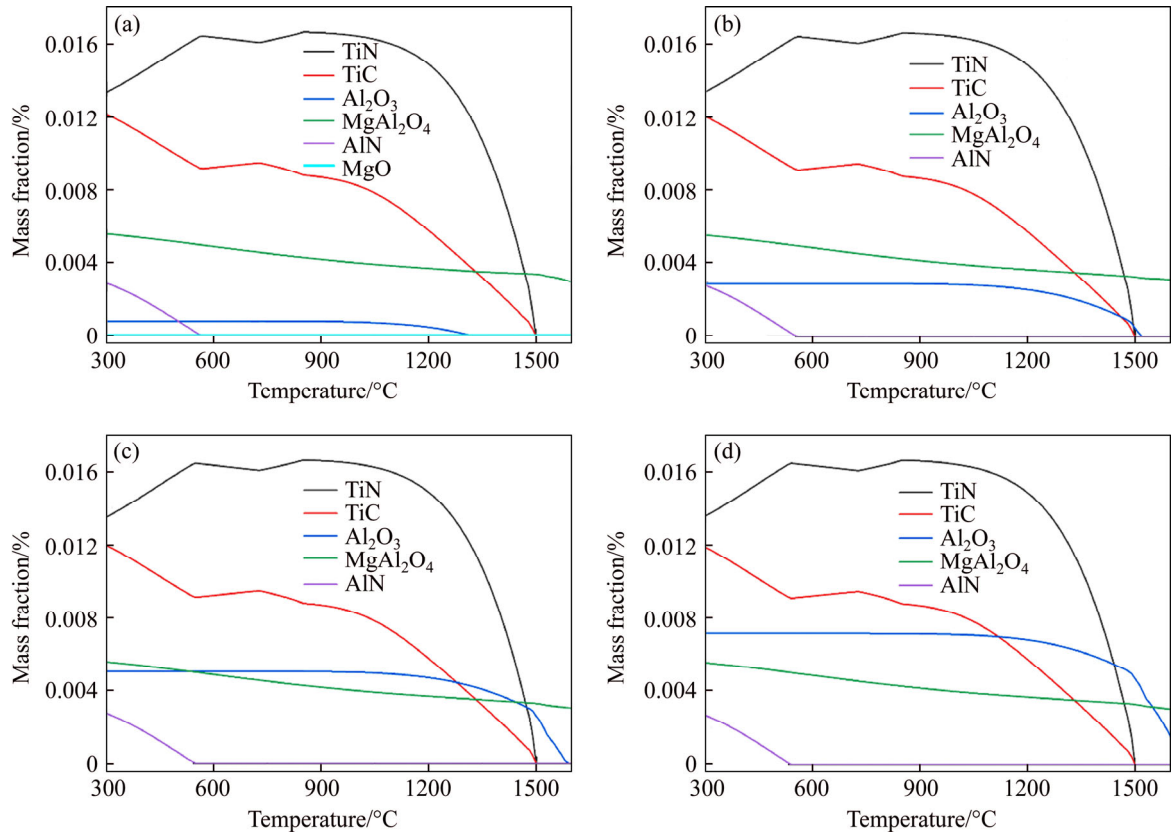

Figure 6 Effect of O content in steel on precipitation behavior of typical precipitates: (a) 30×10^{-6}; (b) 40×10^{-6}; (c) 50×10^{-6}; (d) 60×10^{-6}

temperature molten steel after adding Mg into the Ti-bearing peritectic steel. Based on the induced nucleation mechanism confirmed as mentioned above, these particles provide necessary heterogeneous nucleation sites for refining the high-temperature δ-ferrite, which lays a foundation for the further refinement of original austenite structure.

3.3 Calculations for nitride precipitation during solidification

During solidification, the thermodynamic equilibrium solubilities of solutes in solid phase, which are different from those in liquid phase in the mushy region, cause microscopically the segregation of solute elements at the solidification front. This phenomenon is related to the cooling rate, the equilibrium distribution coefficients of solutes, the counter diffusion rate (i.e., the diffusion coefficients of solutes in solid phase), the rate of dendrite arm coarsening and the dendrite tip undercooling. For these factors, the counter diffusion rate and the rate of dendrite arm coarsening are the two most important factors, which can dilute the liquid phase at the solidification front and should be fully considered in the complete microsegregation model. Some common microsegregation models are Level model [20], Scheil model [20], Brody-Flemings model [20], Ohnaka model [21], Clyne-Kurz model [22, 23] and Voller-Beckmann model [24].

The Level model is an equilibrium solidification model, which assumes that the solutes are fully diffused in both the liquid and solid phases during equilibrium solidification (elements are uniformly distributed in either phase). However, the calculation results of this model are usually not accurate in the later stage of solidification. The Scheil model assumes that the solutes are not diffused in solid phase but fully diffused in liquid phase. It is suitable for the solidification when cooling at an extremely high rate (such as laser welding). The Brody-Flemings model assumes the solutes are fully diffused in liquid phase and partially diffused in solid phase, while the solid-liquid interface is always in a state of dynamic thermal equilibrium:

$$[\%i]_{\mathrm{L}}=[\%i]_0[1+f_{\mathrm{s}}(\beta_i k_i-1)]^{\frac{1-k_i}{\beta_i k_i-1}} \tag{2}$$

where $[\%i]_0$ and $[\%i]_{\mathrm{L}}$ are the mass fractions of element i at the initial time and at the solidification front, respectively; f_{s} is the solid fraction; k_i is the equilibrium distribution coefficient of the element i; β_i is the counter diffusion coefficient, $\beta_i=2\alpha_i$; and α_i is the Fourier series of the solute element i:

$$\alpha_i=\frac{D_{\mathrm{S},i}t_{\mathrm{f}}}{\left(\lambda_{\mathrm{SDAS}}/2\right)^2} \tag{3}$$

where $D_{\mathrm{S},i}$ is the diffusion coefficient of the solute element i in solid phase, for which the specific value is selected according to the literature [25]; t_{f} is the local solidification time; λ_{SDAS} is the secondary dendrite arm spacing, which is a relation with the cooling rate obtained by Won's regression [20]:

$$\lambda_{\mathrm{SDAS}}=319.4R^{-0.378} \tag{4}$$

A correction to the post-diffusion coefficient in the Brody-Flemings model was proposed by Ohnaka based on the assumption that the solutes were quadratically distributed in solid phase:

$$\beta_i=\frac{2\alpha_i}{1+2\alpha_i}\quad\text{or}\quad\beta_i=\frac{4\alpha_i}{1+4\alpha_i} \tag{5}$$

The counter diffusion parameter β_i in the Brody-Flemings model was further corrected by Clyne and Kurz:

$$\beta_i=2\alpha_i\left[1-\exp\left(-\frac{1}{\alpha_i}\right)\right]-\exp\left(-\frac{1}{2\alpha_i}\right) \tag{6}$$

For the one-dimensional microsegregation model, a method was proposed by Voller and Beckermann to consider the effect of dendrite arm coarsening by adding a term to the Fourier number:

$$\alpha_i^{+}=\alpha_i+\alpha^C \tag{7}$$

where α^C is the term added to take the dendrite arm coarsening into consideration. Voller and Beckermann thought that α^C=0.1 could better meet the results of coarsening model under conditions with a wide cooling range.

The local solidification time t_{f} in the above equation is calculated according to the following equation:

$$t_{\mathrm{f}}=\frac{T_{\mathrm{L}}-T_{\mathrm{S}}}{R} \tag{8}$$

where R is the local cooling rate. In fact, different cooling rates also cause the variation of segregation of alloying elements. It was shown in Ref. [20] that

in a given range of cooling rate, the cooling rate had a little effect on the solidus temperature. The solidus and liquidus temperatures of this steel were calculated by Eqs. (9)−(10) [26], and the results were 1794 K for liquidus temperature and 1771 K for solidus temperature:

$$T_{\mathrm{L}}=1809-83\omega[\mathrm{C}]-7.8\omega[\mathrm{Si}]-5\omega[\mathrm{Mn}]-32\omega[\mathrm{P}]-31.5\omega[\mathrm{S}]-1.5\omega[\mathrm{Cr}]-2\omega[\mathrm{Mo}]-2\omega[\mathrm{V}]-3.6\omega[\mathrm{Al}]-18\omega[\mathrm{Ti}] \quad (9)$$

$$T_{\mathrm{S}}=1809-344\omega[\mathrm{C}]-12.3\omega[\mathrm{Si}]-6.8\omega[\mathrm{Mn}]-124.5\omega[\mathrm{P}]-183.5\omega[\mathrm{S}]-1.4\omega[\mathrm{Cr}]-4.1\omega[\mathrm{Al}]-4.3\omega[\mathrm{Ti}] \quad (10)$$

As the solidification proceeds, solute elements are continuously removed from the solid phase to the liquid phase, making the temperature of solidification front decrease gradually. The temperature of solidification front can be calculated through the following equation:

$$T_{\mathrm{L-S}}=T_{\mathrm{f}}-\frac{T_{\mathrm{f}}-T_{\mathrm{L}}}{1-f_{\mathrm{S}}\dfrac{T_{\mathrm{L}}-T_{\mathrm{S}}}{T_{\mathrm{f}}-T_{\mathrm{S}}}} \quad (11)$$

where T_{f}, T_{S}, T_{L} and $T_{\mathrm{L-S}}$ are the melting point of pure iron (1809 K), the solidus temperature, the liquidus temperature and the temperature of solidification front, respectively.

When calculating the redistribution behavior of solute elements at the solidification front during solidification, it is crucial to select a suitable microsegregation model. The calculations in this paper were compared with the above-mentioned microsegregation models for the distributions of Ti and N at the solidification front and the selected cooling rate was 0.1 °C/s. The comparison results are shown in Figure 7. It can be seen that the segregation of [Ti] and [N] in the solid-liquid coexistence zone gets stronger with the increase of solid fraction at the solidification front. When the solid fraction is higher than 0.9, the solute elements are notably enriched at the solidification front. By comparing the six microsegregation models above, it is found that the segregation of solute elements at the solidification front calculated from the Level model is not obvious (as it assumes that the solute elements are completely diffused in solid phase), which is far from the actual situation. The Scheil model assumes that the diffusion rate of solute elements in solid phase is 0, resulting in the strongest segregation of solute

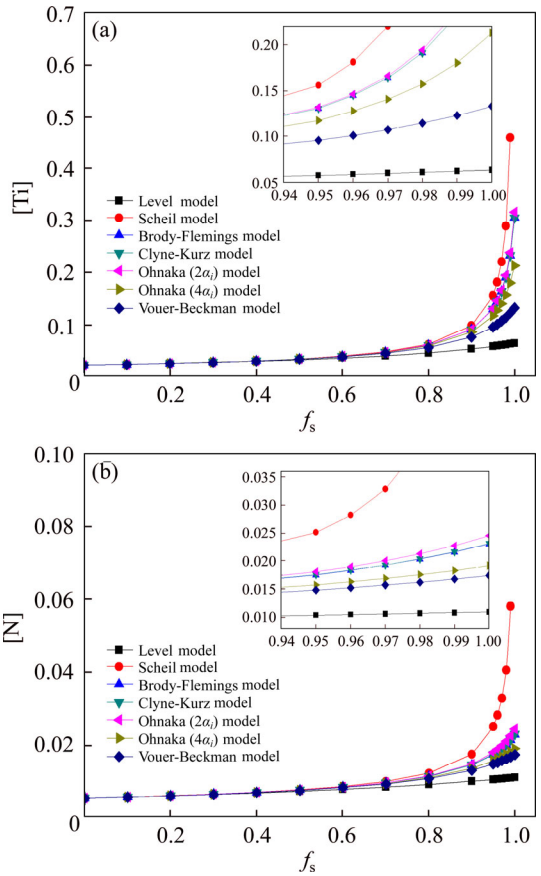

Figure 7 Segregation of [Ti] (a) and [N] (b) at the solidification front

elements at the solidification front. The solid-liquid partition coefficient, k, of Ti is different from that of N, but the enrichment states of solute elements calculated from the Scheil model are similar to each other. Besides, the calculation results of Brody-Flemings, Clyne-Kurz, Vouer-Beckman and Ohnaka models, which all assume the limited diffusion of solute elements in solid phase, are between that of the Level model and the Scheil model, despite that there are a few differences in the results as different manners are adopted by these models to treat the diffusion in solid phase. It can be found that, under the same calculation conditions, the segregation degree of solute elements at the solidification front can be ranked as Scheil> Ohnaka>Brody-Flemings>Clyne-Kurz>Vouer-Beckman>Level. In the calculation process, conditions such as the segregation coefficients of solute elements in the study object and the cooling rate need to be considered when selecting the microsegregation model.

The relationship between the [Ti][N] concentration product at the solidification front and

the solid fraction calculated from different microsegregation models are shown in Figure 8. As the solidification proceeds, TiN particles have precipitated at the solidification front when the solid fraction reaches 0.95 (for the Ohnaka model, the solid fraction needs to reach 0.975), whereas it is manifested by the calculation results of Vouer-Beckman and Level models that no TiN particles were formed before the end of solidification. It is revealed by the sampling of microalloyed steel that the size of TiN particles is much larger than that of NbN particles. The main reason is that the conditions are favorable to both the nucleation and the subsequent growth of TiN particles. Especially in the liquid phase or mushy region, with the help of high melting inclusions (such as MgO, Al_2O_3, $MgAl_2O_4$ particles), the nucleation rate will be remarkably increased.

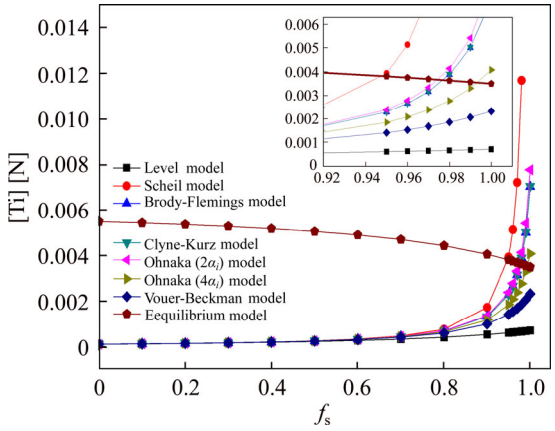

Figure 8 Curve of [Ti][N] concentration product at solidification front against solid fraction

3.4 Appearance characteristics of inclusions in steel

The appearance of TiN particles in the specimens and the distribution of elements before the magnesium treatment are shown in Figure 9, and the appearance and the distribution after the magnesium treatment are shown in Figure 10. As can be seen, the two-dimensional appearance of TiN was a square, and the TiN in specimens with no Mg added mostly existed in pure TiN phase or in a composite phase with Al_2O_3. After Mg was added into the steel, the TiN particles in specimens showed an obvious core. In terms of the core composition, there were generally two types. According to the element distribution diagram, if the Mg and O were evenly distributed in their respective circles, then MgO was considered the core. Similarly, if Mg, O and Al were evenly distributed in their respective circles, the core of TiN was the magnesium-aluminum spinel phase $MgAl_2O_4$. It can be seen that the average size of TiN particles in the specimen before the magnesium treatment was about 4.7 μm, decreased by about 49% to 2.4 μm after the magnesium treatment as shown in Figure 11. If MgO or $MgAl_2O_4$ was taken by TiN in molten steel as the heterogeneous nucleation sites at the beginning of solidification, the required nucleation energy was less. In addition, TiN tended to nucleate on the MgO or $MgAl_2O_4$ surface with a good wet interface, and the nucleation rate was higher. Therefore, a large number of composite TiN particles with MgO or $MgAl_2O_4$ as the cores were formed in the Ti-bearing peritectic steel after the magnesium treatment.

How the grains of Ti-bearing peritectic steel are refined by the magnesium treatment during solidification is shown in Figure 12. After the Mg was added into the Ti-bearing peritectic steel, superfine high-melting inclusions (MgO or $MgAl_2O_4$ particles) rapidly formed with dissolved O and Al in steel. With the decrease of molten steel temperature, the concentration product of [Ti][N] in the molten steel before solidification exceeded the equilibrium concentration product in steel, and then TiN began to precipitate. Due to the good interfacial wettability between TiN and MgO/$MgAl_2O_4$, TiN nucleated on the surface of MgO/$MgAl_2O_4$ particles. When the temperature of molten steel dropped below the liquidus, δ phase began to form from the liquid phase. Similarly, based on the good lattice matching between TiN and δ phase, δ phase was more liable to nucleate on the surface of TiN particles, which promoted the grain refinement of high-temperature δ phase. When the temperature dropped to the peritectic transformation temperature, the peritectic transformation δ+L→γ occurred. Based on the heredity in phase transformation, the refined original austenite structure was obtained, and accordingly, the hot ductility of steel was significantly improved. The refined ferrite structure could also be obtained from the refined original austenite structure during the γ→α phase transformation.

4 Conclusions

1) It is demonstrated by the thermodynamic

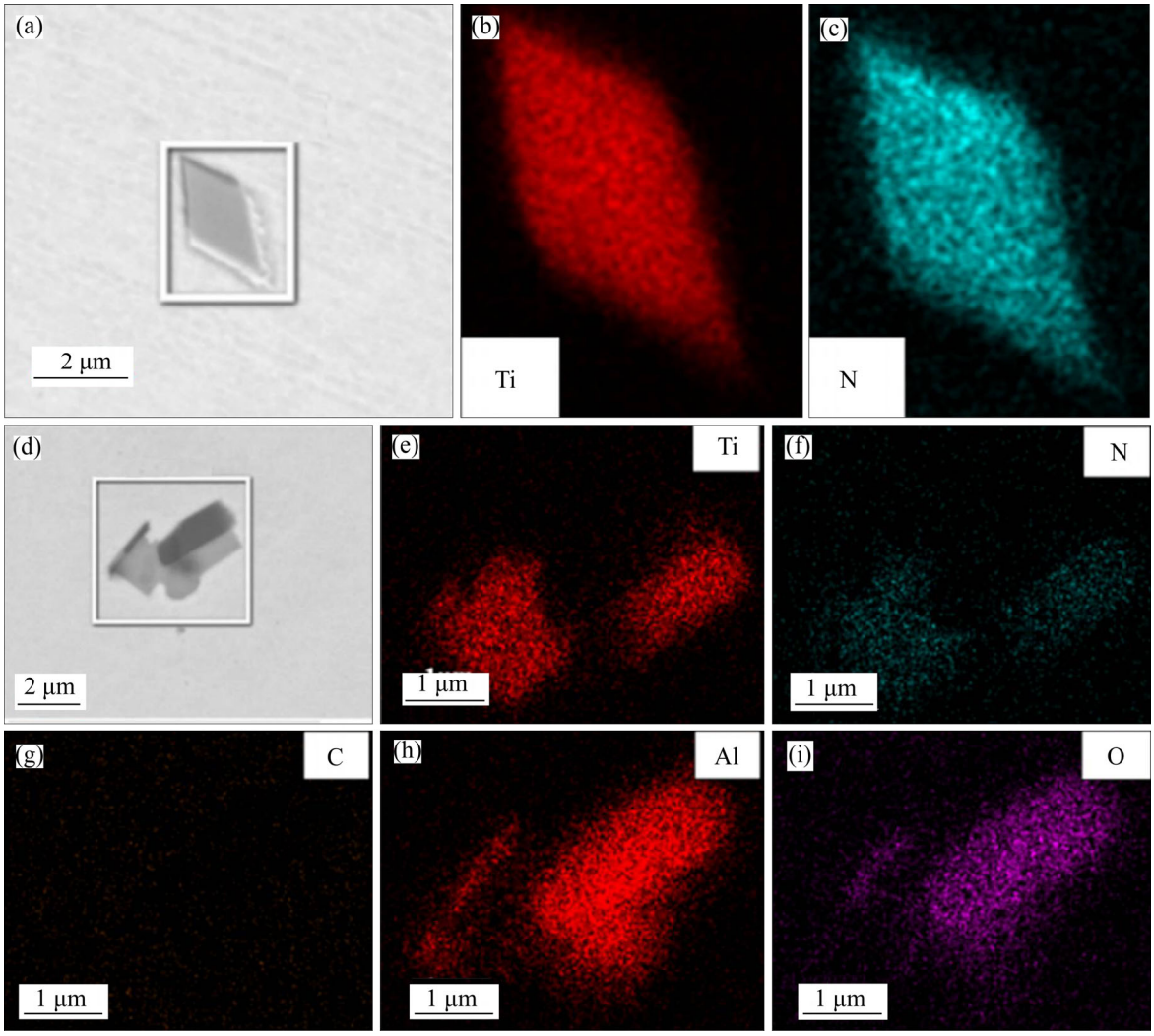

Figure 9 Appearance of TiN particles in specimens before magnesium treatment

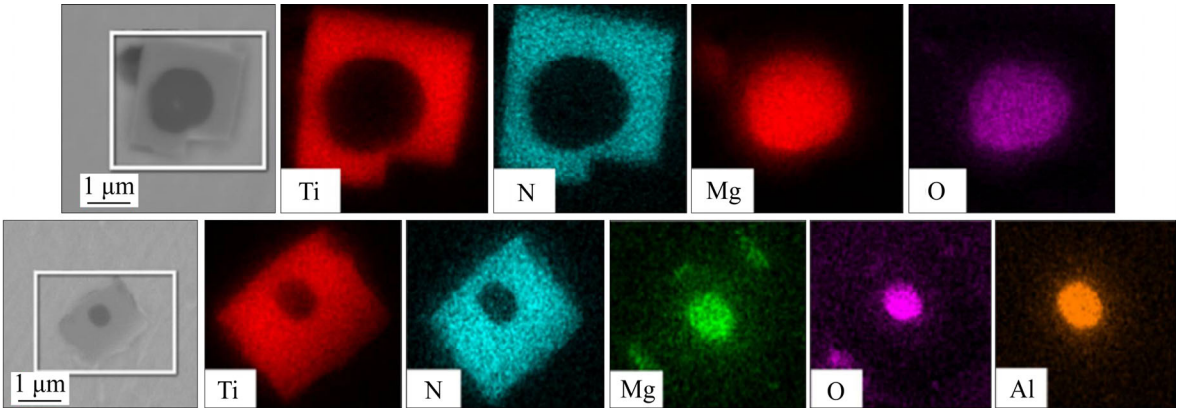

Figure 10 Appearance of TiN particles in specimens after magnesium treatment

calculations that high melting oxide $MgAl_2O_4$ or MgO is always present in the high-temperature molten steel (Ti-bearing peritectic steel) after magnesium treatment, and thus effective nucleation sites to promote the heterogeneous nucleation of TiN are provided.

2) It is shown by the thermodynamic equilibrium calculation results based on the TiN precipitation that TiN does not precipitate in the tested steel until the complete solidification of molten steel, which is inconsistent with the actual situation. The thermodynamic calculation of TiN

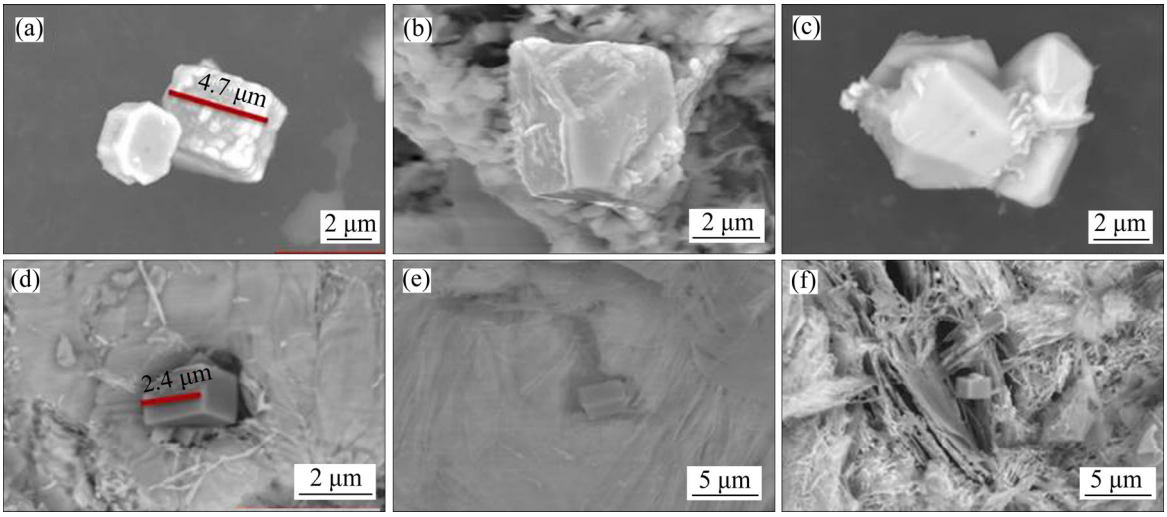

Figure 11 Three-dimensional morphology of typical TiN inclusions: (a−c) Mg free; (d−f) Mg addition

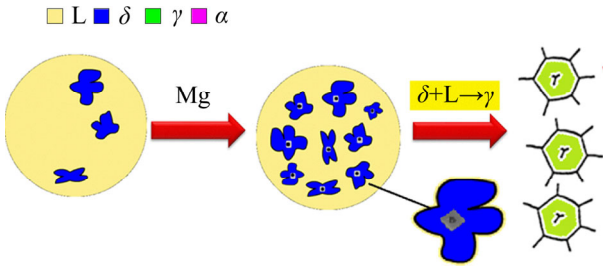

Figure 12 Mechanism of grain size improvement of peritectic steel as a result of magnesium treatment

precipitation needs to consider the segregation and enrichment of solute elements at the solidification front. The Ohnaka microsegregation model was employed to compute the precipitation during solidification. In the event that when the solid fraction reached 0.95 or higher, the concentration product of [Ti][N] at the solidification front exceeded the equilibrium concentration product, and then TiN began to precipitate.

3) It is indicated by the SEM analysis results that MgO or $MgAl_2O_4$ cores were generally found in TiN particles of peritectic steel after the magnesium treatment, which was consistent with the thermodynamic calculation results. Moreover, the average size of TiN particles was reduced by approximately 49%. This reflects that the MgO or $MgAl_2O_4$ particles formed by the magnesium treatment well promoted the heterogeneous nucleation of TiN, and provided nucleation sites for the refinement of high-temperature δ-ferrite.

Contributors

QU Tian-peng and WANG De-yong designed the experiment and the thermal calculation cases. WANG Hui-hua and TIAN Jun analyzed the measured data. The initial draft of the manuscript was written by QU Tian-peng and HOU Dong. All authors replied to reviewers' comments and revised the final version.

Conflict of interest

QU Tian-peng, WANG De-yong, WANG Hui-hua, HOU Dong and TIAN Jun declare that they have no conflict of interest.

References

[1] TAKAHASHI T, OHSASA K, TANAKA J. Peritectic reaction and δ-γ transformation mechanism in carbon steels [J]. Tetsu-to-Hagane, 1987, 73(1): 99−106. DOI: 10.2355/tetsutohagane1955.73.1_99. (in Japanese)

[2] MARUYAMA T, MATSUURA K, KUDOH M, ITOH Y. Peritectic transformation and austenite grain formation for hyper-peritectic carbon steel [J]. Tetsu-to-Hagane, 1999, 85(8): 585−591. DOI: 10.2355/tetsutohagane1955.85.8_585. (in Japanese)

[3] KUDOH M, IGARASHI K, MATSUURA K, OHSASA K. Peritectic transformation in low carbon steels containing high phosphorus concentration [J]. ISIJ International, 2008, 48(3): 334−339. DOI: 10.2355/isijinternational.48.334.

[4] CHEN Hua-biao, LONG Mu-jun, CAO Jun-sheng, CHEN Deng-fu, LIU Tao, DONG Zhi-hua. Phase transition of peritectic steel Q345 and its effect on the equilibrium partition coefficients of solutes [J]. Metals, 2017, 7(8): 288. DOI: 10.3390/met7080288.

[5] GUO Jun-li, WEN Guang-hua, TANG Ping, FU Jiao-jiao, GU Shao-peng. Analysis of crack susceptibility of peritectic steels based on surface roughness [J]. Steel Research International, 2020, 91(2): 1900376. DOI: 10.1002/srin.

201900376.

[6] ALFARO L E, HERRERA T M, RUÍZ M J J, de JESÚS C R M, SOLÍS T H. Effect of C and Mn variations upon the solidification mode and surface cracking susceptibility of peritectic steels [J]. ISIJ International, 2009, 49(6): 851−858. DOI: 10.2355/isijinternational.49.851.

[7] KOROJY B, NASSAR H, FREDRIKSSON H. Hot crack formation during peritectic reaction in steels [J]. Ironmaking & Steelmaking, 2010, 37(1): 63−72. DOI: 10.1179/030192309X12506804200429.

[8] TREJO M H, LOPEZ E A, RUIZ M J J, CASTRO R M D J, TOVAR H S. Effect of solidification path and contraction on the cracking susceptibility of carbon peritectic steels [J]. Metals and Materials International, 2010, 16(5): 731−737. DOI: 10.1007/s12540-010-1006-7.

[9] SALEEM S, VYNNYCKY M, FREDRIKSSON H. The influence of peritectic reaction/transformation on crack susceptibility in the continuous casting of steels [J]. Metallurgical and Materials Transactions B, 2017, 48(3): 1625−1635. DOI: 10.1007/s11663-017-0926-8.

[10] SUZUKI M, HAYASHI H, SHIBATA H, EMI T, LEE I J. Simulation of transverse crack formation on continuously cast peritectic medium carbon steel slabs [J]. Steel Research, 1999, 70(10): 412−419. DOI: 10.1002/srin.199905660.

[11] BRAMFITT B L. The effect of carbide and nitride additions on the heterogeneous nucleation behavior of liquid iron [J]. Metallurgical Transactions, 1970, 1(7): 1987−1995. DOI: 10.1007/BF02642799.

[12] BAKER T N. Microalloyed steels [J]. Ironmaking & Steelmaking, 2016, 43(4): 264−307. DOI: 10.1179/1743281215Y.0000000063.

[13] MORIKAGE Y, OI K, KAWABATA F, AMANO K. Effect of TiN size on ferrite nucleation on TiN in low-C steel [J]. Tetsu-to-Hagane, 1998, 84(7): 510−515. DOI: 10.2355/tetsutohagane1955.84.7_510.

[14] SARMA D S, KARASEV A V, JÖNSSON P G. On the role of non-metallic inclusions in the nucleation of acicular ferrite in steels [J]. ISIJ International, 2009, 49(7): 1063−1074. DOI: 10.2355/isijinternational.49.1063.

[15] KIMURA K, FUKUMOTO S, SHIGESATO G I, TAKAHASHI A. Effect of Mg addition on equiaxed grain formation in ferritic stainless steel [J]. ISIJ International, 2013, 53(12): 2167−2175. DOI: 10.2355/isijinternational.53.2167.

[16] FUKUMOTO S, KIMURA K, TAKAHASHI A. Formation of fine macrostructure in ferritic stainless steel [J]. Tetsu-to-Hagane, 2012, 98(7): 351−357. DOI: 10.2355/tetsutohagane.98.351. (in Japanese)

[17] PARK J S, KIM D H, PARK J H. TEM characterization of a TiN-$MgAl_2O_4$ epitaxial interface [J]. Journal of Alloys and Compounds, 2017, 695: 476−481. DOI: 10.1016/j.jallcom.2016.11.103.

[18] KIM J Y, OH N R, OH Y H, CHO Y T, LEE W B, KIM S K, HONG H U. Hetero-epitaxial nucleation of ferrite at a TiN encapsulating $MgAl_2O_4$ during rapid solidification in a newly developed ferritic stainless steel [J]. Materials Characterization, 2017, 132: 348−353. 10.1016/j.matchar.2017.09.001.

[19] ZHANG Cai-wei, QU Tian-peng, WANG De-yong, TIAN Jun, HOU Dong. Effect of magnesium and titanium composite treatment on solidification structure of stainless steel and its mechanism [J]. Journal of Iron and Steel Research, 2019, 31(7): 661−667. DOI: 10.13228/j.boyuan.issn1001.0963-20180310.

[20] WON Y M, THOMAS B G. Simple model of microsegregation during solidification of steels [J]. Metallurgical and Materials Transactions A, 2001, 32(7): 1755−1767. DOI: 10.1007/s11661-001-0152-4.

[21] OHNAKA I. Mathematical analysis of solute redistribution during solidification with diffusion in solid phase [J]. Transactions of the Iron and Steel Institute of Japan, 1986, 26(12): 1045−1051. DOI: 10.2355/isijinternational1966.26.1045.

[22] CLYNE T W, KURZ W. Solute redistribution during solidification with rapid solid state diffusion [J]. Metallurgical Transactions A, 1981, 12(6): 965−971. DOI: 10.1007/BF02643477.

[23] CLYNE T W, WOLF M, KURZ W. The effect of melt composition on solidification cracking of steel, with particular reference to continuous casting [J]. Metallurgical Transactions B, 1982, 13(2): 259−266. DOI: 10.1007/BF02664583.

[24] VOLLER V R, BECKERMANN C. Approximate models of microsegregation with coarsening [J]. Metallurgical and Materials Transactions A, 1999, 30(11): 3016−3019. DOI: 10.1007/s11661-999-0141-6.

[25] WON Y M, KIM K H, YEO T J, OH K H. Effect of cooling rate on ZST, LIT and ZDT of carbon steels near melting point [J]. ISIJ International, 1998, 38(10): 1093−1099. DOI: 10.2355/isijinternational.38.1093.

[26] CHOUDHARY S K, GHOSH A. Mathematical model for prediction of composition of inclusions formed during solidification of liquid steel [J]. ISIJ International, 2009, 49(12): 1819−1827. DOI: 10.2355/isijinternational.49.1819.

(Edited by ZHENG Yu-tong)

中文导读

镁处理对含 Ti 包晶钢中 TiN 析出行为影响的热力学分析

摘要：含 Ti 钢中普遍存在的 TiN 对钢的力学性能和焊接过程有重要影响，研究 TiN 在冶金熔池中的析出行为有重要意义。本文以含 Ti 包晶钢为研究对象，采用 FactSage 计算了钢种成分对钢中典型夹杂物析出行为的影响规律。采用微观偏析模型对凝固前沿 TiN 的析出过程进行了分析，借助 SEM 对计算结果进行了验证。研究结果表明，镁处理后钢液中始终存在大量弥散分布的高熔点氧化物 $MgAl_2O_4$ 或 MgO，考虑溶质元素在凝固前沿的偏聚富集现象，利用 Ohnaka 微观偏析模型进行凝固析出计算，当固相率达到 0.95 时凝固前沿的[Ti][N]浓度积高于平衡浓度积，开始析出 TiN。镁处理后包晶钢中 TiN 颗粒内部普遍存在 MgO 或 $MgAl_2O_4$ 核心，与热力学计算结果相符，且 TiN 颗粒平均尺寸减小了 62%左右，表明镁处理形成富镁高熔点夹杂物促使了 TiN 异质形核，为进一步细化高温铁素体相提供了有利的形核质点。

关键词：镁处理；包晶钢；TiN；异质形核；热力学分析